International Journal of Sustainable Development and Planning
Vol. 21, No. 7, July, 2026, pp. 2873-2888
Journal homepage: http://iieta.org/journals/ijsdp

Calibration Interval Scenario Modeling for CA-ANN Prediction of Land Cover Change in a Tropical Watershed Ecosystem: A Case Study of Nagari Muaro Sungai Lolo, West Sumatra, Indonesia

Yudi Antomi[1*], Dian Adhetya Arif[2], Dilla Angraina[2], Kurnia Anggraini[3]

[1] Department of Remote Sensing and GIS, Vocational College and Environmental Science Studies, Universitas Negeri Padang, Padang 25132, Indonesia
[2] Department of Remote Sensing and GIS, Vocational College, Universitas Negeri Padang, Padang 25132, Indonesia
[3] Department of Geography, Faculty of Mathematics and Natural Sciences, Universitas Indonesia, Depok 16424, Indonesia

Corresponding Author Email: antomi_y@fis.unp.ac.id

https://doi.org/10.18280/ijsdp.210701

Received: 9 April 2026
Revised: 8 June 2026
Accepted: 20 June 2026
Available online: 31 July 2026

Keywords:
calibration interval scenario, land cover change, tropical watershed, Sumatra, deforestation prediction, spatial simulation, Figure of Merit

ABSTRACT

Land cover change in tropical watershed ecosystems poses critical threats to biodiversity, hydrological integrity, and regional carbon stocks. While Cellular Automata–Artificial Neural Network (CA-ANN) models have advanced land-cover prediction, the influence of calibration-interval selection on model reliability remains systematically unexplored—particularly in complex tropical highland landscapes. This study introduces and validates a calibration interval scenario framework for CA-ANN prediction of land-cover change, applied to Nagari Muaro Sungai Lolo, Pasaman Regency, West Sumatra, Indonesia (00°06'N–00°34'N; 100°06'E–100°20'E), a critical upstream watershed supplying the Koto Panjang Hydroelectric Power Plant (HEPP). Multi-temporal Landsat 8 and 9 imagery for 2016, 2020, and 2024 was processed on Google Earth Engine (GEE) using the Classification and Regression Trees (CART) algorithm, achieving Overall Accuracy (OA) of 86.7%, 83.4%, and 93.35% (Kappa: 0.86, 0.79, 0.87) respectively. Land cover analysis documented a net plantation expansion of +2,249% (+418 ha), a +733% increase in built-up land (+139 ha), and accelerating deforestation during the 2020–2024 sub-period (−1.56%/year), against a backdrop of near-total agricultural land collapse (−94.9%). Three calibration interval scenarios (S1: 2016–2020; S2: 2016–2024; S3: 2020–2024) were evaluated using the Figure of Merit (FoM), Quantity Disagreement (QD), and Allocation Disagreement (AD). The 8-year interval (S2) was adopted for the 2030 and 2034 forecasts because it spans the full multi-phase transition trajectory of the landscape. Topographic variables (slope gradient: importance 0.89; elevation: 0.82) dominated transition potential, followed by distance to roads (0.74). Projections to 2030 and 2034 indicate continued forest loss (−8.3% and −14.1% relative to 2024) and sustained plantation and urban expansion. These results directly support Sustainable Development Goal (SDG) 13 and SDG 15 targets and provide a replicable calibration optimization framework for CA-ANN modeling in tropical watersheds globally.

1. INTRODUCTION

Land cover change is among the most consequential processes reshaping the structure and functioning of the Earth's terrestrial ecosystems. Globally, more than 1.5 million km² of forest cover were lost between 2000 and 2020, with tropical forests bearing the greatest burden of this transformation [1, 2]. Such changes fundamentally disrupt ecosystem services, including carbon sequestration, freshwater regulation, biodiversity conservation, and regional climate stabilization [3-5]. In Southeast Asia, the confluence of population growth, agricultural intensification, plantation development, and infrastructure expansion has produced some of the highest rates of land cover change on Earth [6-8]. Indonesia, which harbors the third-largest tropical forest globally, has experienced annual forest loss averaging 500,000–700,000 ha, concentrated in Sumatra, Kalimantan, and Papua [9, 10]. These losses carry profound implications for biodiversity, climate regulation, and the Sustainable Development Goals (SDGs) that Indonesia has committed to achieving.

Reliable spatial prediction of future land-cover states, rather than retrospective monitoring alone, is essential to support proactive environmental governance and evidence-based spatial planning. The integration of satellite remote sensing, Geographic Information Systems (GIS), and spatial simulation models has substantially advanced the capability to quantify and project land cover dynamics across large extents and temporal scales [11-13]. Among predictive modeling approaches, Cellular Automata (CA) models are widely valued for their capacity to represent spatially explicit, local-rule-governed transition dynamics [14, 15]. The integration of

Artificial Neural Networks (ANNs) into CA frameworks, yielding the Cellular Automata–Artificial Neural Network (CA-ANN) hybrid, has substantially improved predictive accuracy by enabling data-driven learning of the complex, non-linear interaction patterns that drive land-cover transitions in heterogeneous tropical landscapes [16-19]. Comparative studies have consistently demonstrated the superiority of CA-ANN over logistic regression, basic Markov chains, and multi-criteria evaluation approaches in capturing multidimensional transition dynamics [20-22].

Despite significant methodological progress, critical gaps persist in the CA-ANN literature. The most consequential yet consistently neglected issue is the sensitivity of CA-ANN predictions to the calibration interval, the temporal window used to train the ANN transition potential model. The calibration interval fundamentally determines the land cover transitions from which the ANN learns spatial associations with driver variables. A calibration period that does not adequately represent the structural transition dynamics of the landscape may produce systematically biased transition potentials, either over-representing temporary perturbations or under-representing emergent trends, leading to substantial prediction errors that propagate through the simulation [23-25]. Remarkably, the overwhelming majority of published CA-ANN studies apply a single, arbitrarily chosen calibration interval without systematic evaluation of alternative temporal configurations or quantification of the sensitivity of predictions to interval selection [17, 26-28]. This methodological gap constitutes an underappreciated source of structural uncertainty in CA-ANN-based land-cover projections.

A second major research gap concerns the geographic context of existing studies. The vast majority of CA-ANN applications are situated in urban-periurban fringe environments, cultivated lowlands, or semi-arid regions where land cover dynamics are relatively straightforward and driver-transition relationships are well-characterized [29-31]. Tropical highland watersheds characterized by complex and steep topography, dense multi-strata vegetation communities, high endemic biodiversity, and critical hydrological roles in regional water supply remain severely underrepresented in the CA-ANN literature, despite constituting some of the most ecologically and socioeconomically critical landscapes affected by land cover change globally [32, 33]. In Indonesia specifically, CA-ANN studies are sparse and geographically concentrated in Java and coastal North Sumatra [26, 27]. leaving the complex highland watersheds of West Sumatra essentially uncharacterized in terms of spatial land cover change modeling.

The Nagari Muaro Sungai Lolo watershed in Pasaman Regency, West Sumatra Province, represents a critically important yet unstudied landscape in this context. Located at the headwaters of the Kampar River, this area constitutes the primary upstream catchment zone supplying the Koto Panjang Hydroelectric Power Plant (HEPP) reservoir, a strategically important energy infrastructure serving West Sumatra and Riau provinces. The landscape is characterized by extreme topographic relief (elevation range: 150–2,281 m asl), high-diversity tropical montane and sub-montane forests, and a dynamic agricultural frontier dominated by shifting cultivation, rubber and cocoa agroforestry, and rapidly expanding plantation development [34]. Critical land in Pasaman Regency has expanded from 69,718 ha to 154,512 ha in a single year [35], signaling acute and accelerating pressure on land degradation. Despite this vulnerability, no spatially explicit land-cover prediction model has been developed for this watershed.

This study addresses these intersecting gaps by advancing the evaluation of calibration interval sensitivity in CA-ANN modeling. While previous studies have explored the influence of calibration periods on simulation performance, few have systematically tested multiple calibration scenarios within a unified analytical framework, and such evidence remains limited for tropical highland watershed environments, particularly in West Sumatra. First, it introduces a systematic calibration interval scenario framework for CA-ANN modeling, in which multiple temporal calibration configurations are explicitly defined, executed, and evaluated against standardized accuracy metrics, including Figure of Merit (FoM), Quantity Disagreement (QD), and Allocation Disagreement (AD), to identify the optimal calibration configuration for predictive simulation. Second, it generates high-accuracy multi-temporal land cover maps for 2016, 2020, and 2024 using Classification and Regression Trees (CART) classification on GEE and quantifies land cover transitions and their spatial drivers in the Nagari Muaro Sungai Lolo watershed. Third, it applies the optimal calibration scenario to project land cover change in 2030 and 2034, providing an evidence-based spatial foundation for watershed conservation, forest management, and regional spatial planning. The research thereby advances both the methodological state-of-the-art in CA-ANN spatial modeling and the empirical knowledge base for sustainable land use governance in Indonesia's highland watersheds.

2. METHOD

2.1 Study area

Nagari Muaro Sungai Lolo is located in Mapat Tunggul Selatan Sub-district, Pasaman Regency, West Sumatra Province, Indonesia, as shown in Figure 1. The area spans 00°06'N–00°34'N and 100°06'E–100°20'E. The research area represents a portion of Nagari Muaro Sungai Lolo, covering approximately 124.72 km² (12,472 ha), corresponding to the delineated watershed analysis extent rather than the full administrative area. The eastern boundary of the Nagari directly adjoins Riau Province. The study area encompasses the headwaters of the Lolo River, a principal tributary of the Kampar River system and the primary hydrological source for the HEPP reservoir, an infrastructure of significant national energy security importance (Figure 1).

Topographically, the area is highly heterogeneous, with elevations ranging from 150 m to 2,281 m above sea level, producing diverse ecological gradients from lowland riparian forests to montane cloud forest communities. Mean annual precipitation ranges from approximately 2,200 mm to 3,500 mm [36], classified as a tropical rainforest climate (Köppen–Geiger Af). The resident population is approximately 4,200 inhabitants. BPS Mapat Tunggul Selatan Sub-district [37] practices predominantly subsistence agriculture, including shifting cultivation on approximately 1,455 ha and irrigated rice farming on 354 ha. Agroforestry systems producing cocoa, rubber, cassava, and areca nut have been established on slopes of 30–40° within formally designated protected forest zones [38]. The area falls within the jurisdiction of the Governor of West Sumatra Regulation No. 45/2013, which designates approximately 42% of the Koto Panjang watershed drainage area within Pasaman Regency as a priority water catchment zone.

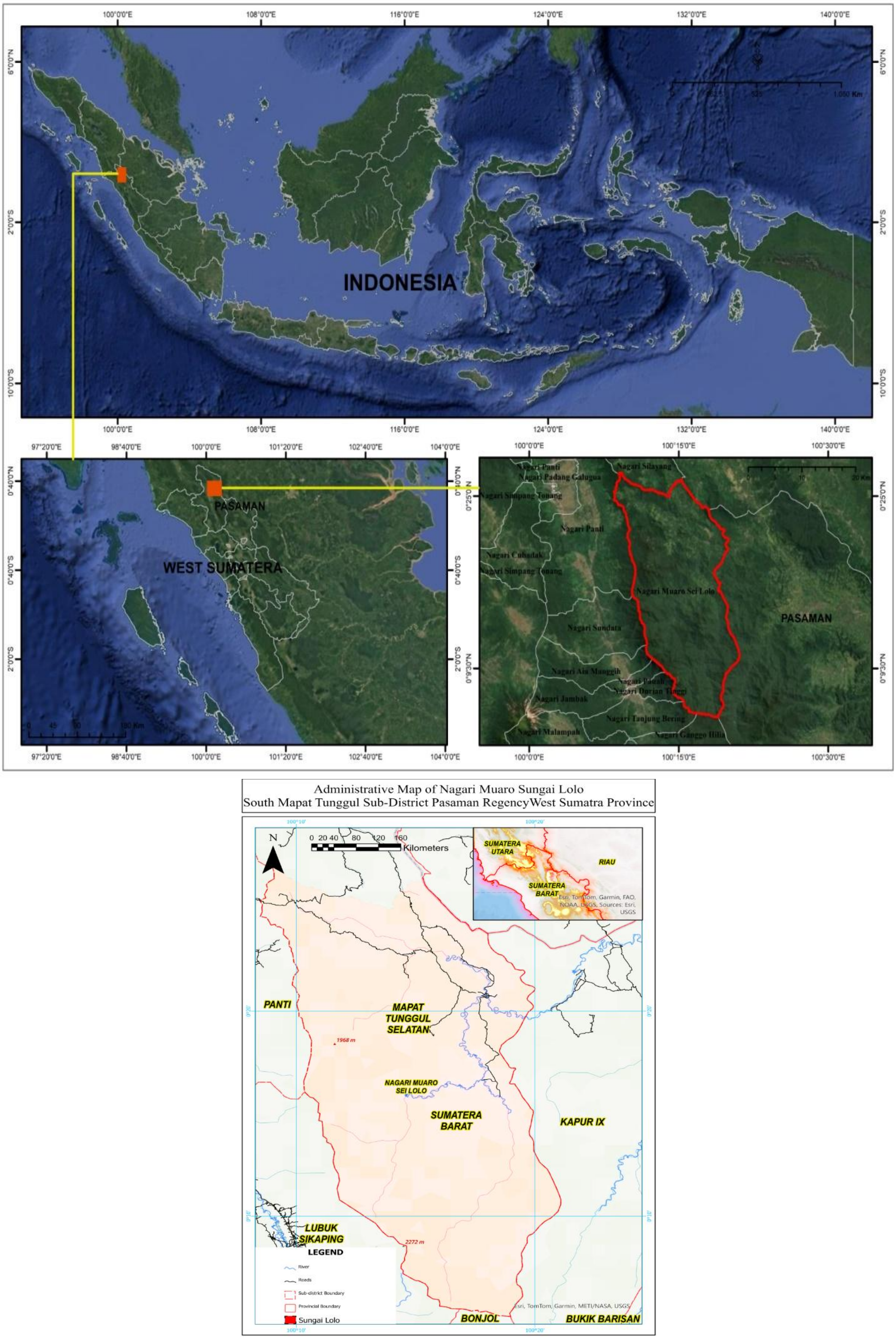

Figure 1. Study site

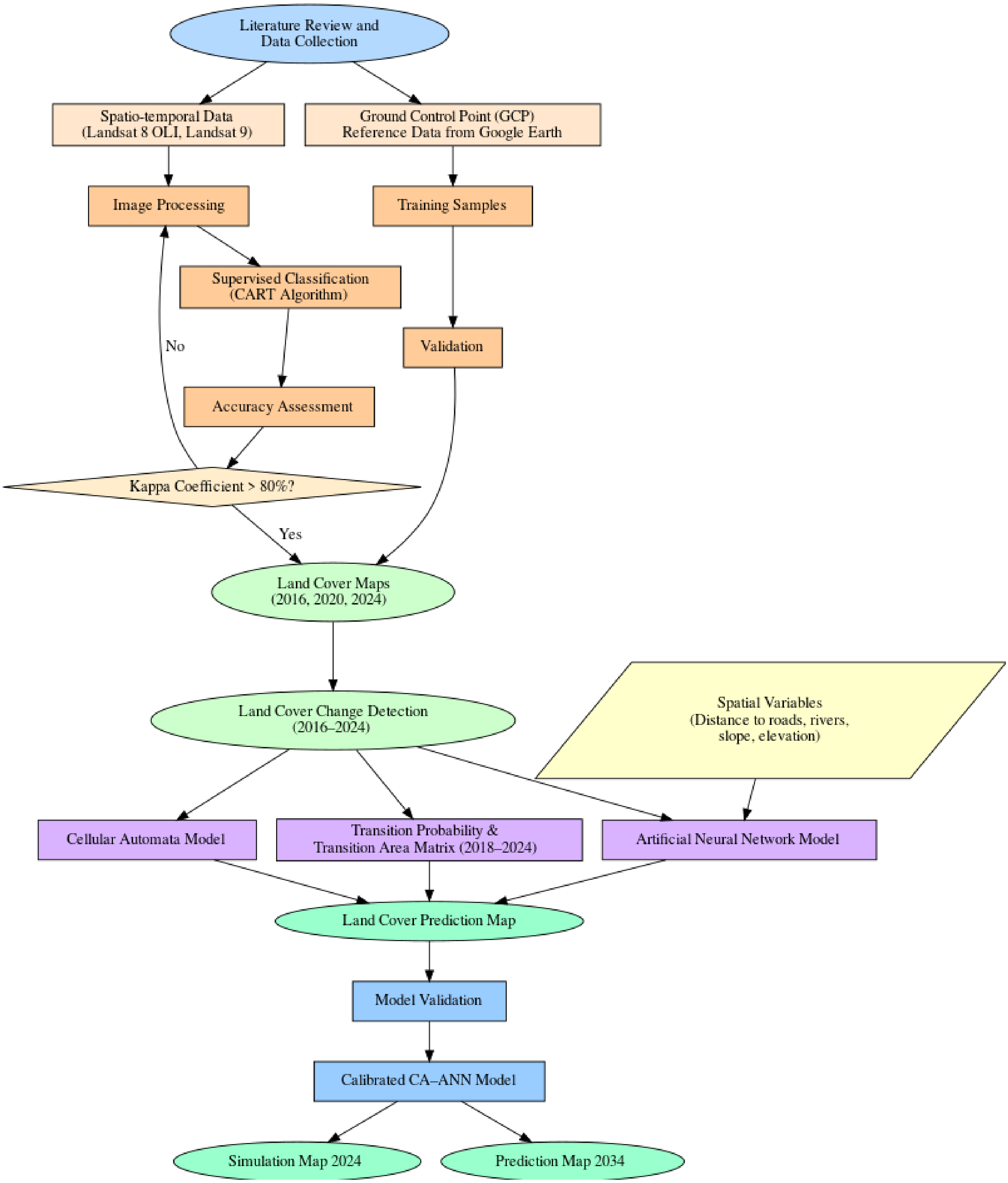

Figure 2. Workflow

Table 1. Remote sensing datasets used in this study

Sensor	Epoch	Resolution	Spectral Bands	Product Level
Landsat 8 OLI	2016, 2020	30 m	B2–B7, NDVI, NDBI	USGS Collection 2 SR
Landsat 9 OLI-2	2024	30 m	B2–B7, NDVI, NDBI	USGS Collection 2 SR
SRTM DEM	Static	30 m	Elevation, Slope	NASA/USGS v3
CHIRPS v2.0	2016–2024	~5.5 km (resampled)	Annual precipitation	UCSB Climate Hazards
OpenStreetMap	2024	Vector	Road network	OSM Contributors

2.2 Remote sensing data and preprocessing

Multi-temporal land cover classification was based on Landsat imagery sourced from the Google Earth Engine (GEE) data catalog (Table 1). Landsat 8 Operational Land Imager (OLI) Collection 2 Level-2 surface reflectance products were used for the 2016 and 2020 epochs, while Landsat 9 OLI-2 Collection 2 Level-2 products were used for the 2024 epoch. Both sensors provide 30 m spatial resolution multispectral imagery across six reflective bands (Blue B2, Green B3, Red B4, NIR B5, SWIR1 B6, SWIR2 B7), with a 16-day revisit period [39]. Surface reflectance products incorporate LaSRC atmospheric corrections and terrain illumination normalization (Figure 2) [40, 41].

The methodological workflow of this study is illustrated in Figure 2, which presents the sequence of analytical stages applied in the research, starting from satellite data preprocessing and land cover classification to the preparation of spatial driver variables and the implementation of the CA-ANN modeling framework. As part of the preprocessing stage, cloud masking was performed using the CFmask algorithm through the QA_PIXEL quality band to eliminate pixels affected by clouds, cloud shadows, and snow or ice. To ensure consistent and reliable imagery for each observation year, annual cloud-free composite images were produced by applying median pixel compositing over the full acquisition period from January 1 to December 31, following recommended practices for cloud-persistent tropical regions [42]. The spectral variables used for classification consisted of six reflective Landsat bands together with two widely applied spectral indices, namely the Normalized Difference Vegetation Index (NDVI = [B5 − B4] / [B5 + B4]) and the Normalized Difference Built-up Index (NDBI = [B6 − B5] / [B6 + B5]), which enhance the differentiation between vegetation, built-up areas, and other land cover types (Table 1).

2.3 Land cover classification using the Classification and Regression Trees algorithm

Supervised land cover classification was performed in GEE using the CART algorithm, selected for its interpretability, robustness to outliers, and demonstrated performance in multi-spectral tropical land cover mapping [13, 43, 44]. Six land cover classes were defined, following the Indonesian National Standard SNI 7645-1:2014 and adapted to the KLHK classification scheme: (1) Forest, (2) Plantation, (3) Mixed Crops/Agriculture, (4) Built-up Land, (5) Bare Land, and (6) Water Bodies.

Training and validation samples were collected using a stratified random sampling strategy with density proportional to class area and landscape heterogeneity [45]. A total of 450 reference points were collected across all epochs, corresponding to 25 samples per class for each of the six land cover classes, in each of the three observation years (150 points per epoch of the years 2016, 2020, and 2024), through visual interpretation of high-resolution Google Earth Pro imagery, corroborated by field survey records and BPS village statistics (Table 2). Because 25 points per class do not divide evenly at a 70/30 ratio, the split was applied to the pooled reference set of 450 points, producing 315 training points and 135 independent validation points (i.e., 105 training and 45 validation points per epoch). Per-class reference totals are therefore uniform (25 per class per epoch); per-class training/validation counts follow the pooled random split and are not stratified within class. CART hyperparameters were optimized via 5-fold cross-validation: minimum leaf size = 10; maximum tree depth = 15.

Table 2. Distribution of reference points

Land Cover Class	Points of Epoch 2016, 2020, 2024	Total
Forest	25	75
Plantation	25	75
Mixed Crops/Agr	25	75
Built up Land	25	75
Bare Land	25	75
Water Bodies	25	75
Total	150	450
Training/Validation (70/30)	105/45 per Epoch	315/135

Accuracy was assessed using the standard confusion matrix framework, computing Overall Accuracy (OA), Producer's Accuracy (PA), User's Accuracy (UA), and the Kappa coefficient. Area estimates were calculated using the stratified area estimator [46]. Additionally, a Receiver Operating Characteristic (ROC) analysis was conducted for each class to evaluate discrimination capacity across classification probability thresholds, and the FoM was computed at the classification stage for each epoch.

2.4 Spatial driver variables

Five spatial driver variables were prepared as continuous 30 m raster layers, co-registered to the Landsat grid (WGS84/UTM Zone 47N; Table 3). The selection of these variables was guided by established studies on drivers of land-cover transitions in Indonesian tropical landscapes [26, 27, 47, 48]. The variables include (1) slope gradient (degrees), derived from the SRTM DEM using the Horn algorithm; (2) elevation (m asl), obtained from the SRTM DEM; (3) Euclidean distance to roads (m), calculated from the OpenStreetMap road network; (4) Euclidean distance to rivers (m), derived from the national hydrological network; and (5) mean annual rainfall (mm), averaged from CHIRPS v2.0 data for the period 2016–2024. Before model input, all raster layers were normalized to a range between 0 and 1 to ensure comparability among variables. The spatial distribution of the main topographic and accessibility-related driver variables used in the modeling process is illustrated in Figure 3, including elevation, distance to roads, slope gradient, and distance to rivers (Figure 3 and Table 3).

2.5 Cellular Automata–Artificial Neural Network modeling framework

A spatially explicit land cover change simulation was conducted using the CA-ANN approach implemented in the Modules for Land Use Change Evaluation (MOLUSCE) plugin v3.0.2 in QGIS 3.22, following established protocols [16, 17]. The framework integrates two components: (1) a Multi-Layer Perceptron ANN that learns spatial associations between land cover transitions and driver variables, producing class-specific transition potential surfaces; and (2) a CA engine that applies these potentials iteratively over a spatial grid using defined neighborhood rules.

The MLP-ANN architecture consisted of one hidden layer, with the neuron count optimized over the range 10–40 in 5-

neuron increments using 5-fold cross-validation (optimal: 20 neurons). A sigmoid activation function was applied, with backpropagation and momentum optimization. The learning rate was set to 0.001 after adaptive tuning, with a maximum of 10,000 iterations and a convergence threshold of 0.001. The CA component used a 5 × 5 Moore neighborhood kernel with one-year iteration steps. Model performance was evaluated using the FoM:

$$FoM = |Observed\ Change \cap Simulated\ Change| \,/\, |Observed\ Change \cup Simulated\ Change|$$

QD and AD are calculated to decompose the overall model disagreement into its quantity and spatial allocation components [23]. These three metrics together provide a comprehensive characterization of the quality of CA-ANN predictions.

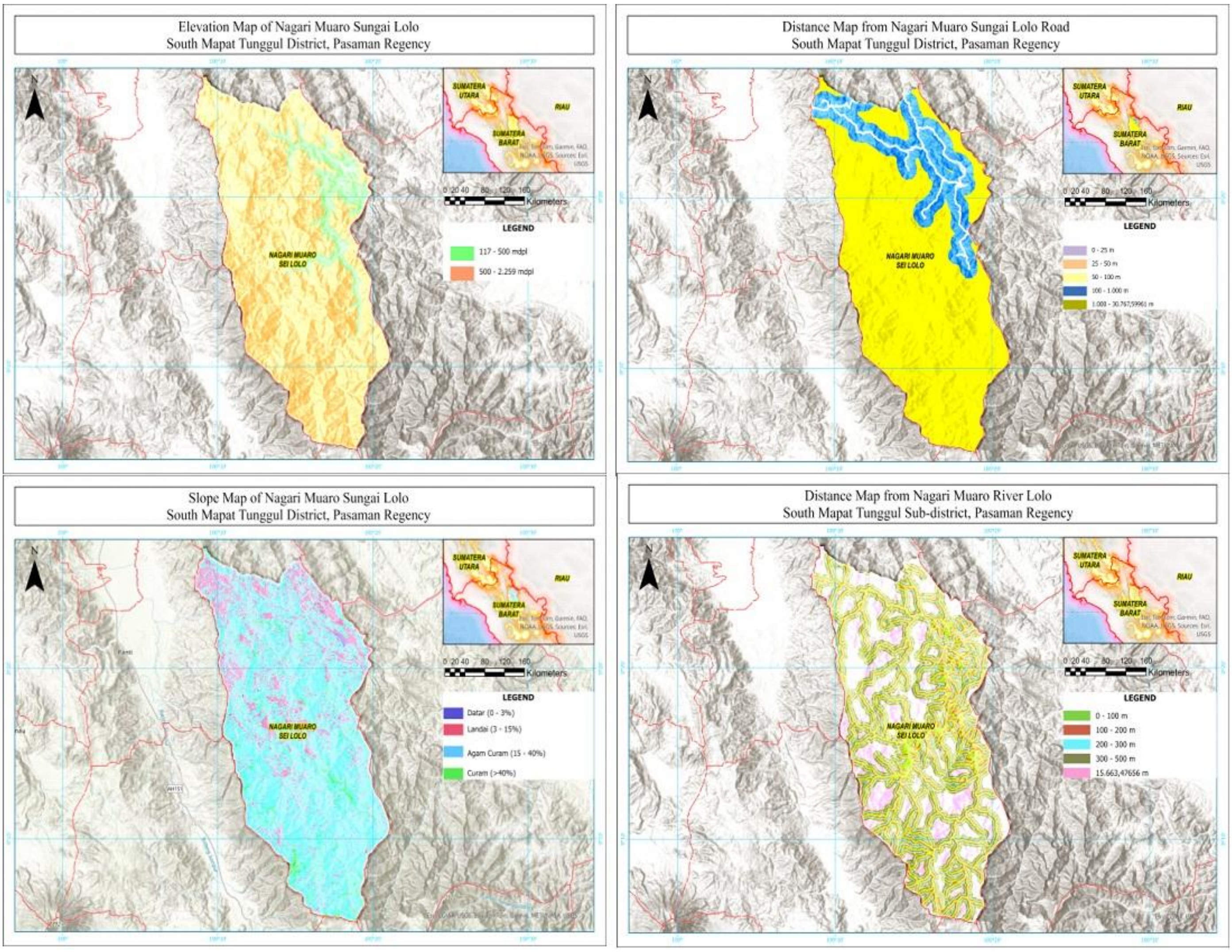

Figure 3. Elevation, distance from roads, slope gradient, and distance from rivers

Table 3. Spatial driver variables, sources, and ecological rationale

No.	Variable	Source	Resolution	Ecological Rationale
1	Slope Gradient (°)	SRTM DEM v3	30 m	Limits accessibility and cultivation suitability
2	Elevation (m asl)	SRTM DEM v3	30 m	Controls vegetation zonation and agro-climatic feasibility
3	Distance to Roads (m)	OpenStreetMap	30 m (rasterized)	Proximate driver of forest frontier encroachment
4	Distance to Rivers (m)	National Hydro Network	30 m (rasterized)	Governs riparian agriculture and settlement patterns
5	Annual Rainfall (mm)	CHIRPS v2.0	~5.5 km → 30 m	Determines moisture availability for land use transitions

Table 4. Calibration interval scenarios systematically evaluated in this study

Scen.	T1 (Base)	T2 (Cal. End)	T3 (Validation)	Interval	Design Rationale
S1	2016	2020	2024	4 yr	Short window: independently validated against the observed 2024 map
S2	2016	2024	2030*	8 yr	Long window: spans the full structural transition trajectory (used for projection)
S3	2020	2024	2030*	4 yr	Recent window: captures contemporary plantation expansion (projection comparison)

Note: * = projection target; no observed validation data available.

2.6 Calibration interval scenario design

The central methodological innovation of this study is the systematic evaluation of calibration interval scenarios. The calibration interval defines the temporal training window used by the ANN to infer land-cover transition patterns. Three scenarios were designed based on the three available classification epochs (Table 4).

Scenario S1 (2016-2020 → 2024) was constructed as a temporally independent validation scenario. In this sequence, the 2024 land cover map was the validation target, and the simulation was assessed using FoM, QD, AD, and Validation OA. Conversely, Scenarios S2 and S3 were projection-oriented scenarios, implemented to analyze the effect of different calibration intervals on future land-cover forecasting to 2030, given the absence of validation data at that horizon. The projection using S2 was then carried out for 2030 and 2034 using the classified 2024 map as the starting point of the simulation. This framework separates the independently validated simulation (S1) from the forward-looking projection scenarios (S2, S3).

3. RESULTS AND DISCUSSION

3.1 Classification accuracy assessment

CART classification achieved high accuracy across all three epochs (Table 5). The 2016 map attained OA = 86.7% and Kappa coefficient (K) = 0.86; the 2020 map achieved OA = 83.4%, K = 0.79; and the 2024 map achieved the highest accuracy at OA = 93.35%, K = 0.87. All values exceed or approach the minimum operational threshold of 85% OA [49, 50] and are consistent with published CART-GEE classification performance in analogous tropical environments [43]. The marginal reduction in accuracy in 2020 reflects an elevated residual cloud fraction in the annual composite despite CFmask filtering. Improvements in 2024 reflect the superior signal-to-noise ratio of Landsat 9 OLI-2 and optimized sample collection. Bare Land consistently achieved 100% UA across all epochs due to its spectrally distinct signature. PA for Plantation improved markedly from 82.4% (2016) to 91.5% (2024), reflecting increasing class area and improved separability as plantations matured (Table 5).

3.2 Multi-temporal land cover change analysis (2016–2024)

Land cover analysis reveals substantial and multi-directional transformation of the Nagari Muaro Sungai Lolo landscape over the eight-year observation period (Table 6). The spatial distribution of land cover for the three observation years is presented in Figure 4, which illustrates the classified land cover maps for 2016, 2020, and 2024. Forest remained the dominant cover type throughout the study period, although its trajectory showed notable fluctuations. Forest area increased from 9,814.69 ha in 2016 to 11,199.84 ha in 2024, representing a net gain of 1,385.15 ha over the full observation period. This overall increase was driven by a substantial rise between 2016 and 2020, when forest expanded to 11,822.88 ha (+20.5%), which may partly reflect improved classification accuracy due to enhanced cloud masking, the reclassification of agroforestry areas previously misidentified as other land cover types, and natural regeneration on abandoned agricultural land. However, this trend reversed during the 2020–2024 period, with forest declining by 623.04 ha (−5.3%), indicating localized deforestation with an estimated annual rate of −1.56%. This pattern suggests that while the long-term trend indicates net forest gain, deforestation pressures occurred during the later observation period (Figure 4).

Agricultural land experienced the most dramatic transformation, declining from 2,398.42 ha (2016) to 128.62 ha (2020), a loss of 94.6% in four years before stabilizing at 121.66 ha (2024). This near-total collapse reflects the large-scale abandonment of traditional shifting cultivation and conversion to plantation agriculture and fallow bare land. Plantation cover exhibited the most consistent and striking expansion, growing from 18.58 ha (2016) to 436.58 ha (2024), a 2,249% increase equivalent to 52.3 ha/year average expansion. Built-up land increased from 18.93 ha (2016) to a peak of 181.97 ha (2020), then declined to 157.75 ha (2024), suggesting active settlement growth followed by spatial consolidation.

Table 5. Classification accuracy assessment results for all epochs

Land Cover Class	PA 2016	PA 2020	PA 2024	UA 2024	UA 2020	Accuracy Trend
Forest	88.2	85.1	94.3	96.1	87.3	Consistently high; improved 2024
Plantation	82.4	79.3	91.5	89.7	81.2	Improving the class area increases.
Mixed Crops/Agriculture	84.6	81.0	93.8	91.3	83.5	Stable; spectral confusion with fallow
Built-up Land	91.3	88.6	95.2	94.5	90.1	High across all epochs
Bare Land	100.0	95.4	100.0	100.0	100.0	Spectrally distinct; excellent
Water Bodies	90.5	87.3	92.1	93.4	88.7	Good; seasonal variation noted
Overall Accuracy (%)	86.70	83.40	93.35	—	—	Peak in 2024 (Landsat 9)
Kappa Coefficient	0.86	0.79	0.87	—	—	Substantial to almost perfect

Note: PA = Producer's Accuracy; UA = User's Accuracy.

Table 6. Land cover area statistics and change metrics, 2016–2024

Land Cover	2016 (ha)	2020 (ha)	2024 (ha)	Δ 2016–2024 (ha)	Δ (%)	Rate (ha/yr)
Forest	9,814.69	11,822.88	11,199.84	+1,385.15	+14.1	+173.1
Mixed Crops/Agric.	2,398.42	128.62	121.66	−2,276.76	−94.9	−284.6
Plantation	18.58	89.72	436.58	+418.00	+2,249	+52.3
Built-up Land	18.93	181.97	157.75	+138.82	+733.6	+17.4
Bare Land	196.76	202.98	510.34	+313.58	+159.4	+39.2
Water Bodies	24.62	45.83	45.83	+21.21	+86.2	+2.7
Total Study Area	12,472	~12,472*	12,472	—	—	—

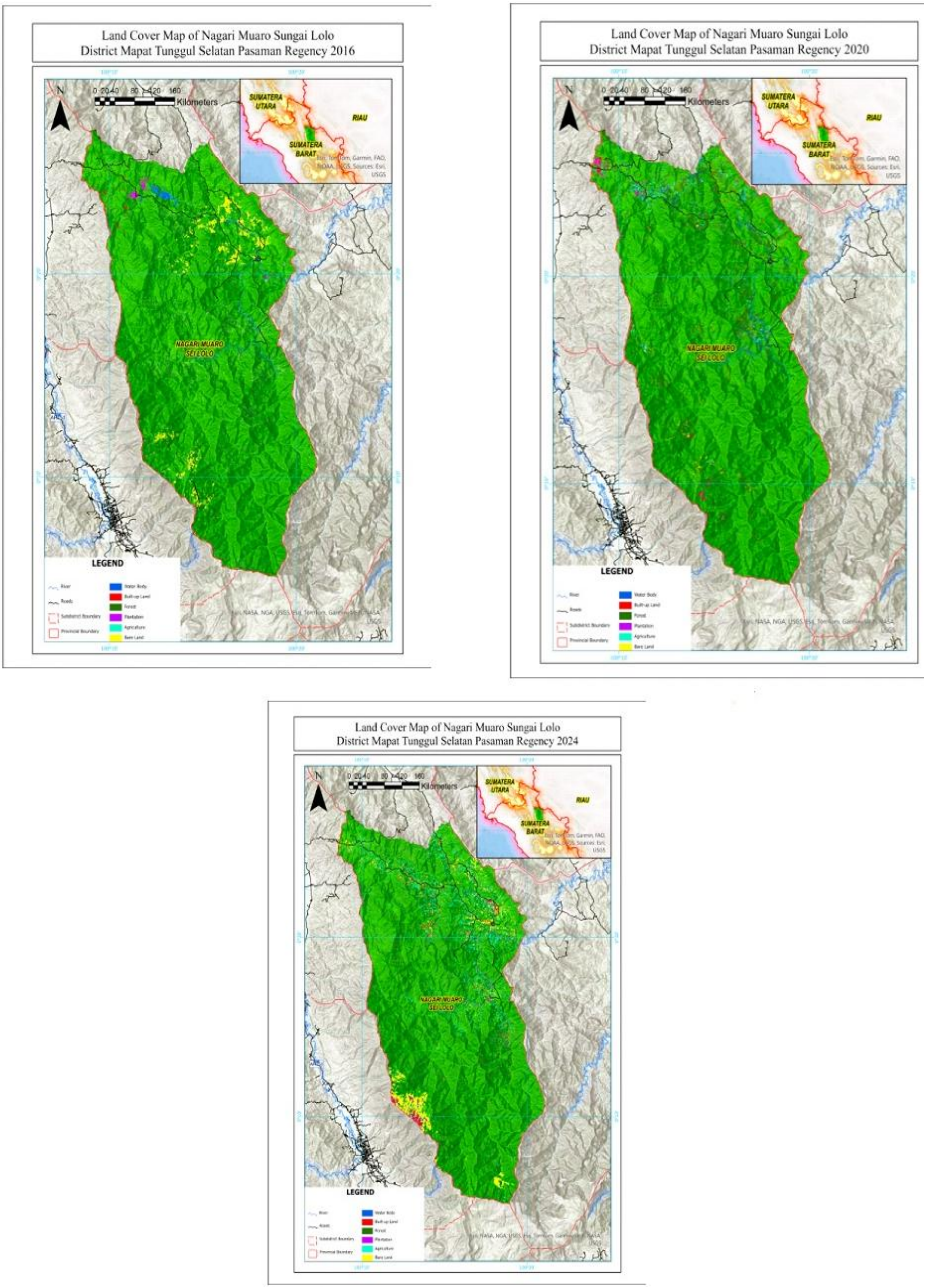

Figure 4. Land cover maps for 2016, land cover maps for 2020, and land cover maps for 2024

Bare land increased persistently from 196.76 ha (2016) to 510.34 ha (2024), a 159.4% expansion indicative of ongoing land clearing and soil exposure during plantation establishment cycles. Water bodies increased moderately from 24.62 ha to 45.83 ha (+86.2%) (Table 6).

3.3 Land cover transition matrix (2016–2024)

The cross-tabulation transition matrix (Table 7) revealed the dominant conversion pathways driving landscape transformation between 2016 and 2024. The single largest gross transition was Agricultural land → Forest: 1,888.65 ha (78.7% of the original agricultural area), reflecting the widespread abandonment of shifting cultivation and subsequent vegetative regrowth and reclassification to forest, which accounted for the net forest gain recorded in the early 2016–2020 period. The principal degradation pathways, concentrated in the later 2020–2024 period, were: (1) Agricultural land → Plantation: 308.4 ha (12.9% of the original agricultural area), documenting direct conversion from food crops to commodity perennial crops; (2) Forest → Bare Land: 295.79 ha (3.0% of the original forest area), representing land clearing that had not yet been converted to a productive land use by 2024; and (3) Forest → Plantation: 120 ha (1.2% of the original forest area), representing direct deforestation for plantation establishment. The spatial distribution of these major land cover transitions is illustrated in Figure 5, highlighting the areas where the most significant landscape transformations occurred during the study period (Figure 5).

Stable areas (diagonal entries) were dominated by Forest (9,300.3 ha), confirming that the majority of forest area remained intact, with change concentrated at accessible topographic positions. The largest single stable class after Forest was Bare Land (196.07 ha), indicating the persistence of degraded sites over the eight years (Table 7).

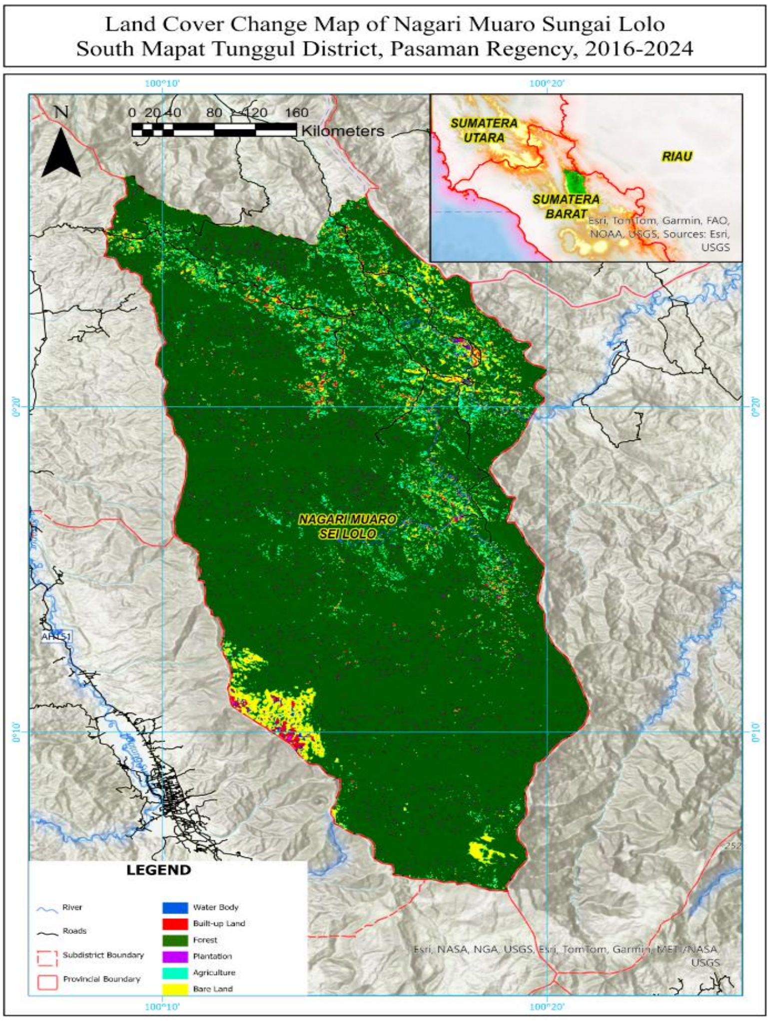

Figure 5. Spatial distribution of major land cover transitions between 2016 and 2024

Table 7. Land cover transition matrix, 2016–2024 (values in hectares; diagonal = stable classes)

2016 → 2024	Forest	Plantation	Agriculture	Built-Up	Bare Land	Water
Forest	9,300.3	120	9.5	86.7	295.79	2.7
Plantation	4.3	8.18	6.1	8.3	0.0	0.0
Agriculture	1888.65	308.4	106.06	58.32	15.16	21.83
Built-up	6.2	0.0	0.0	12.73	0.0	0.0
Bare Land	0.69	0.0	0.0	0.0	196.07	0.0
Water	0.1	0.0	0.0	0.0	3.32	21.3

Note: Green-shaded diagonal cells indicate stable land-cover areas. Off-diagonal = gross transition areas (ha).

3.4 Calibration interval scenario performance evaluation

Different calibration interval scenarios produced distinct simulation characteristics and projection behaviors (Table 8). Scenario S1 (2016–2020 calibration; 2024 validation) quantified performance with a FoM of 0.31, QD of 0.13, AD of 0.19, and showed independent validation OA of 81.2%, all of which represent acceptable simulation performance for a temporally independent validation.

Table 8. Calibration interval scenario configurations and validation status

Scenario	Calibration Period	Validation Status	Purpose
S1	2016–2020	Validated using observed 2024 map (FoM = 0.31; OA = 81.2%)	Independent validation scenario
S2 ★	2016–2024	Projection only (no observed target map)	Long-term structural trajectory projection
S3	2020–2024	Projection only (no observed target map)	Recent transition dynamics projection

Note: FoM = Figure of Merit, OA = Overall Accuracy.

Subsequent scenarios, S2 (2016–2024) and S3 (2020–2024), were implemented as more projection-centric calibration scenarios for land-cover simulations towards 2030 where validation data are, as of yet, non-existent. Among the two, Scenario S2 was chosen for the longer calibration interval, containing multiple phases of land-use transition and thus requiring more structural representation of the landscape for the ANN to generalize the upcoming shifts in land use [24, 25]. Scenario S3, on the other hand, was more confined to the plantation expansion phase and short-term dynamics. Therefore, Scenario S2 was used to cover all land-cover projections.

3.5 Spatial driver variable importance

ANN connection-weight analysis for the Scenario S2 model revealed a clear hierarchical importance of the five driver variables across all transition sub-models (Table 9). Slope gradient was the most influential driver (normalized importance score: 0.89), confirming the dominant role of topographic accessibility as both a constraint on and determinant of land cover change in this mountainous watershed. Elevation ranked second (0.82), capturing altitudinal vegetation zonation and the practical limits of mechanized agriculture. Distance to roads ranked third (0.74), reflecting the role of road infrastructure in opening forest frontiers to encroachment and settlement expansion. Distance to rivers ranked fourth (0.61), governing riparian agriculture and settlement concentration in valley bottoms. Annual rainfall ranked lowest (0.43), likely because spatial variation in precipitation within the uniformly wet study area is insufficient to strongly differentiate transition potentials (Table 9).

Table 9. Normalized Artificial Neural Network (ANN)-derived importance scores for spatial driver variables (Scenario S2)

Rank	Driver Variable	Importance Score	Key Ecological Mechanism
1	Slope Gradient (°)	0.89	Primary topographic barrier to agricultural encroachment and forest clearing
2	Elevation (m asl)	0.82	Controls vegetation type, agro-climatic feasibility, and accessibility altitude thresholds
3	Distance to Roads (m)	0.74	Infrastructure access drives the opening of forest frontiers and the expansion of settlement.
4	Distance to Rivers (m)	0.61	Riparian agriculture concentration; regulatory buffer zone constraints
5	Annual Rainfall (mm)	0.43	Marginally discriminating in a uniformly high-precipitation tropical setting.

3.6 Land cover projections for 2030 and 2034

Application of the Scenario S2 model parameters to the 2024 baseline map yielded projections for 2030 and 2034 (Table 10; Figure 6(a) and (b)). Forest area is projected to decline from 11,199.84 ha (2024) to 10,268.4 ha (2030) and 9,617.6 ha (2034), representing cumulative losses of 931.4 ha (−8.3%) and 1,582.2 ha (−14.1%), respectively, relative to 2024, at an average annual rate of 158.2 ha/year. Plantation area is projected to expand continuously from 436.58 ha (2024) to 651.82 ha (2030) and 829.46 ha (2034), a +90% increase (+392.88 ha) over the projection period. Built-up land is projected to grow from 157.75 ha (2024) to 243.68 ha (2030) and 336.41 ha (2034), an increase of +178.66 ha (+113.3%) over the projection period. Bare land is projected to increase substantially and continuously, from 510.34 ha (2024) to 1,134.89 ha (2030) and 1,531.24 ha (2034), a +200% expansion (+1,020.9 ha), reflecting sustained land clearing during ongoing plantation establishment. Mixed crops/agriculture continues its gradual decline (−9.8% by 2034), suggesting continued substitution by plantation monocultures (Table 10).

Table 10. Projected land cover areas for 2030 and 2034 under the selected calibration scenario (S2)

Land Cover Class	2024 (ha)	2030 (ha)	2034 (ha)	Δ 2024–2034 (ha)	Δ (%)	Trend
Forest	11,199.84	10,268.4	9,617.6	−1,582.2	−14.1	↓
Plantation	436.58	651.82	829.46	+392.88	+90	↑
Mixed Crops/Agric.	121.66	117.34	109.72	−11.9	−9.8	↓
Built-up Land	157.75	243.68	336.41	+178.66	+113.3	↑
Bare Land	510.34	1,134.89	1,531.24	+1,020.9	+200	↑
Water Bodies	45.83	56.87	47.57	+1.74	+3.8	~
Deforestation Rate	Baseline	−1.38%/yr	−1.56%/yr	Avg. −1.55%/yr	—	↓↓

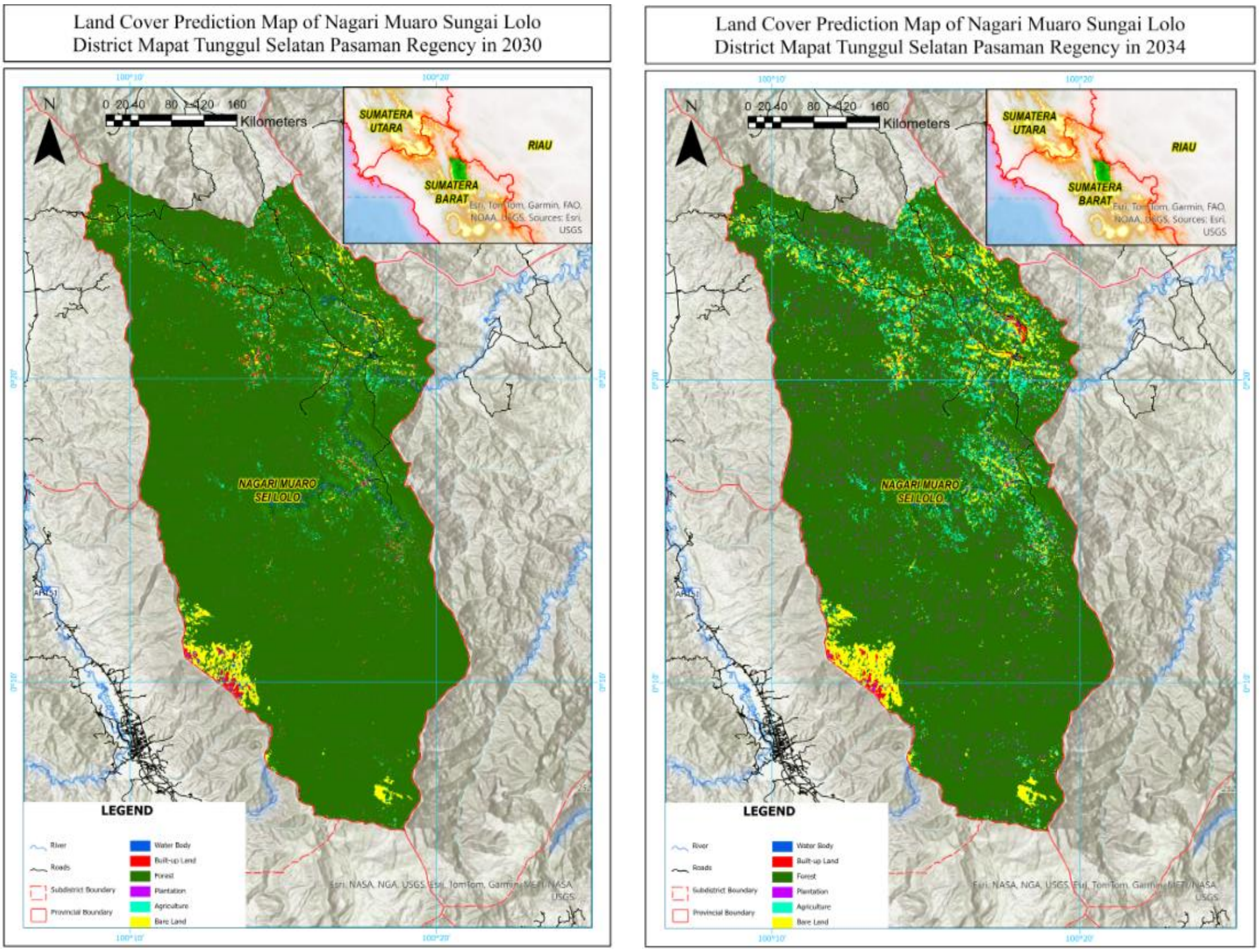

(a) (b)

Figure 6. Projected land cover for the years 2030 and 2034

3.7 Discussion

3.7.1 Drivers of deforestation and land cover change

The land cover dynamics documented in this study reflect the interaction of three dominant socioeconomic drivers operating at multiple scales: (1) plantation agriculture expansion, (2) infrastructure development, and (3) the transformation of traditional shifting cultivation systems. The near-total collapse of agricultural land (−94.9% over 2016–2024), accompanied by a 2,249% increase in plantations and a 159% increase in bare land, signals a fundamental structural shift from subsistence-oriented to commodity-oriented land use in the Lolo watershed. This transition parallels the broader pattern of smallholder-driven commodity expansion (rubber, cocoa, and increasingly oil palm) documented across highland Sumatra [8, 51, 52].

The identification of slope gradient as the primary transition driver (importance score 0.89) aligns with findings from analogous Indonesian contexts [27, 47]. It confirms that topographic accessibility is the fundamental constraint governing the spatial distribution of land cover change in this mountainous watershed. The concentration of observed transitions in areas with slopes below 4° and elevations below 100 m is consistent with the transition matrix, which shows that, alongside the extensive reversion of abandoned agricultural land to forest, the principal degradation flows were the conversion of forest and agricultural land to bare land and plantation, reflecting well-established principles of agricultural suitability and mechanization thresholds in tropical highlands [48, 53]. The persistence of forest on steeper slopes (>25°) represents a de facto protection mechanism that may be eroded as frontier populations seek new cultivation areas under demographic and economic pressure [54].

Road proximity ranked third in importance (0.74), consistent with extensive evidence that road infrastructure is the proximate driver of tropical deforestation by reducing extraction costs and increasing accessibility [55-57]. The substantial expansion of built-up land (+733% over 2016–2024) indicates active infrastructure development, including road improvements and village expansion, that is creating new forest access corridors in previously inaccessible upland areas. River proximity (rank 4; importance 0.61) governs the concentration of agricultural and settlement activity in valley bottoms and is directly relevant to the enforcement of riparian buffer zone regulations (Regulation No. 28/PRT/M/2015), which restrict development within defined distances from water bodies.

3.7.2 Methodological significance of calibration interval scenario modeling

The calibration interval scenario framework introduced in this study offers a practical addition to conventional CA-ANN practice. Systematic evaluation of multiple calibration windows against standardized accuracy metrics remains uncommon in the CA-ANN literature, and we are aware of no such assessment for tropical highland watersheds in West Sumatra; most applications adopt a single calibration period without reporting sensitivity to that choice [16, 17, 26-28, 58]. In this study, only S1 could be validated against an observed target map (the 2024 classification, FoM = 0.31, validation OA = 81.2%); S2 and S3, whose calibration windows end at the last observed epoch, have no hold-out year and are therefore used as projection settings rather than validated configurations. The framework's contribution is thus a reproducible procedure for defining and comparing calibration windows, not a validated ranking of them.

The choice of the 8-year window (S2) for projection rests on the theoretical expectation that longer calibration periods better capture the structural transition trajectory of a landscape, reducing the risk of conflating phase-specific dynamics with permanent structural change [24, 25]: the 2016–2024 window encompasses both the agricultural-collapse phase (2016–2020) and the plantation-expansion phase (2020–2024), whereas the 2020–2024 window (S3) is confined to the latter. This is a design-based rationale; it is not a claim of measured predictive superiority, because S2 and S3 cannot be validated against an observed future map.

For context, published FoM values include 0.24 for Chunati Wildlife Sanctuary, Bangladesh [16]; 0.29–0.33 for a Jordanian urban landscape [17]; 0.27 for Makassar City, Indonesia [26]; and 0.28–0.33 in Malaysia [58]. The validated scenario in this study (S1, FoM = 0.31) is comparable to these benchmarks. Because the scenario comparison requires no additional data acquisition, it is a low-cost step that makes the influence of calibration-interval choice explicit rather than leaving it as an untested assumption.

3.7.3 Comparison with studies from Indonesia, Southeast Asia, and tropical regions

The deforestation dynamics documented in this study are broadly consistent with patterns reported from comparable Indonesian and Southeast Asian highland watersheds. The researcher [47] documented similar topographic control of deforestation in East Kalimantan, with steeper slopes exhibiting significantly lower deforestation pressure, consistent with our slope importance finding (0.89). Another researcher reported CA-ANN-based projections for North Sumatra [27] showing sustained forest loss driven by plantation expansion, with OA values of 82–88% comparable to our results. In peninsular Malaysia, the researchers [58] documented plantation-driven deforestation in protected area buffer zones using CA-ANN, finding that road proximity was the primary driver of encroachment, aligning with our results. In Brazil's Amazon basin, the researchers [59, 60] documented similar multi-driver land cover dynamics with annual deforestation rates of 0.8–2.5%/year in frontier zones, within which our projected 2024–2034 rate of 1.55%/year sits as a significant but not extreme trajectory. In sub-Saharan Africa, the researchers [61] documented comparable topographically controlled land-cover change in Ethiopian highland watersheds, with agricultural expansion and road access identified as principal drivers, reinforcing the cross-regional generality of the topographic-accessibility-plantation nexus documented in this study.

3.7.4 Implications for watershed conservation and regional policy

The projected continued deforestation of 1,582 ha by 2034 in the Kampar River headwater zone carries critical implications for the hydrological integrity of the Koto Panjang HEPP watershed. Extensive evidence from comparable tropical montane catchments documents that forest loss increases peak discharge, annual sediment yield, and flood frequency [62, 63]. Accelerated reservoir sedimentation from upstream deforestation threatens the long-term operational capacity and power-generation efficiency of the Koto Panjang HEPP, a strategically important energy infrastructure asset for the West Sumatra and Riau provinces. This risk warrants the urgent integration of watershed land-cover projections into HEPP operational management planning.

The results of this study directly support SDGs 13 (Climate Action) and 15 (Life on Land) by quantifying the climate and biodiversity costs of projected land-cover change and providing a spatial evidence base for intervention prioritization. The projected forest loss of 1,582 ha by 2034, at a conservative aboveground biomass carbon density of 150 Mg C/ha [64, 65], corresponds to an estimated committed carbon emission of approximately 870,210 Mg CO_2e, equivalent to the annual emissions of approximately 50,000 automobiles. Preventing this deforestation through proactive watershed conservation represents a direct, measurable contribution to Indonesia's updated Nationally Determined Contribution (NDC) targets under the Paris Agreement [66], which commit to 31.89% greenhouse gas emission reductions unconditionally and up to 43.20% with international support by 2030.

The topographic concentration of transition pressure on low-gradient, low-elevation zones provides a spatially explicit targeting opportunity for conservation interventions. Regulatory buffer zones along rivers under Regulation No. 28/PRT/M/2015, combined with targeted reforestation incentives on slopes of 15–30° where transition potential is highest under the S2 projection, could substantially reduce the projected forest loss. The strong road-deforestation nexus underscores the need to integrate road expansion planning with environmental impact assessment under RTRW spatial planning regulations to prevent unintended forest fragmentation. The spatial transition probability maps generated by the CA-ANN model can directly inform priority area identification for REDD+ interventions within the Pasaman Regency spatial plan (RTRW Kabupaten Pasaman) and Indonesia's Social Forestry programs.

3.8 Limitations and future research

This study acknowledges several limitations that should guide future research. First, driver variables were held static throughout the 2024–2034 projection period, not accounting for future road expansion, demographic change, or policy interventions. Future studies should incorporate dynamic driver scenarios derived from road network expansion models and infrastructure development plans. Second, Landsat's 30 m resolution may underestimate fine-scale plantation and agroforestry conversion in highly fragmented landscapes; future applications should evaluate Sentinel-2 (10 m) for improved sub-pixel change detection. Third, while this study employed FoM-based scenario comparison, a full ensemble or Monte Carlo uncertainty quantification for projection confidence intervals was not conducted; this is a methodological priority for future work. Fourth, socioeconomic drivers (land tenure security, commodity prices, governance capacity) were not explicitly modeled;

their integration as dynamic inputs into the CA-ANN framework represents a significant frontier for advancing the explanatory and predictive power of spatial land cover change models in data-constrained tropical settings.

4. CONCLUSIONS

This study made original contributions across three dimensions: scientific, methodological, and policy-relevant. Scientifically, it delivered the comprehensive spatial prediction of land-cover change for the Nagari Muaro Sungai Lolo watershed, a critical yet previously uncharacterized tropical highland catchment supplying the HEPP. High-accuracy CART-GEE classification (OA: 86.7–93.35%; K: 0.79–0.87) documented profound landscape transformation over 2016–2024: plantation expansion of +2,249% (+418 ha), built-up land growth of +733% (+139 ha), near-total agricultural collapse (−94.9%), and accelerating deforestation at −1.56%/year in 2020–2024. Topographic variables (slope and elevation) were identified as the dominant transition drivers, with road proximity third, confirming that the accessibility-topography interaction governs the spatial pattern and pace of land cover change in this mountainous watershed.

Methodologically, the study introduced and applied a calibration interval scenario framework for CA-ANN modeling. Of the three configurations, only S1 (2016–2020 calibration) could be independently validated against the observed 2024 map (FoM = 0.31, validation OA = 81.2%). The 8-year window (2016–2024, S2) was adopted for projection because it best represents the full structural transition trajectory of the landscape; as no observed 2030 map exists, S2 was not validated and no ranking of scenarios by predictive performance is claimed. The framework nonetheless makes calibration-interval selection an explicit, reproducible modeling decision rather than an untested default. This framework is fully reproducible using open-source tools (GEE, QGIS-MOLUSCE) and is generalizable to any landscape with three or more classified temporal maps. Its adoption as standard practice would substantially improve the rigor and reliability of CA-ANN-based land cover projections globally.

From a policy perspective, projections to 2030 (−8.3% forest) and 2034 (−14.1% forest) relative to 2024, corresponding to ≈ 870,210 Mg CO_2e committed emissions, provide actionable spatial intelligence for watershed conservation and climate mitigation planning. The spatial probability maps generated by the model enable prioritized REDD+ area identification and targeted enforcement of riparian buffer zones, directly supporting SDG 13 and SDG 15 targets and Indonesia's NDC commitments.

Future research priorities include: (1) integration of dynamic driver scenarios incorporating road expansion and infrastructure development trajectories; (2) application of Sentinel-2 (10 m) imagery for improved sub-pixel classification; (3) ensemble-based uncertainty quantification for projection confidence intervals; and (4) incorporation of socioeconomic drivers as dynamic model inputs to advance the explanatory completeness of spatial land cover change prediction in tropical highland settings.

ACKNOWLEDGMENT

The Research Team appreciates and is most grateful to Universitas Negeri Padang for conducting this research.

REFERENCES

[1] Hansen, M.C., Wang, L., Song, X.P., et al. (2020). The fate of tropical forest fragments. Science Advances, 6(11): eaax8574. https://doi.org/10.1126/sciadv.aax8574

[2] Turubanova, S., Potapov, P.V., Tyukavina, A., Hansen, M.C. (2018). Ongoing primary forest loss in Brazil, Democratic Republic of the Congo, and Indonesia. Environmental Research Letters, 13(7): 074028. https://doi.org/10.1088/1748-9326/aacd1c

[3] Song, X.P., Hansen, M.C., Stehman, S.V., et al. (2018). Global land change from 1982 to 2016. Nature, 560(7720): 639-643. https://doi.org/10.1038/s41586-018-0411-9

[4] Erb, K.H., Kastner, T., Plutzar, C., et al. (2018). Unexpectedly large impact of forest management and grazing on global vegetation biomass. Nature, 553(7686): 73-76. https://doi.org/10.1038/nature25138

[5] Foley, J.A., DeFries, R., Asner, G.P., et al. (2005). Global consequences of land use. Science, 309(5734): 570-574. https://doi.org/10.1126/science.1111772

[6] Miettinen, J., Stibig, H.J., Achard, F. (2014). Remote sensing of forest degradation in Southeast Asia: Aiming for a regional view through 5–30 m satellite data. Global Ecology and Conservation, 2: 24-36. https://doi.org/10.1016/j.gecco.2014.07.007

[7] Estoque, R.C., Ooba, M., Avitabile, V., et al. (2019). The future of Southeast Asia's forests. Nature Communications, 10(1): 1829. https://doi.org/10.1038/s41467-019-09646-4

[8] Wilcove, D.S., Giam, X., Edwards, D.P., Fisher, B., Koh, L.P. (2013). Navjot's nightmare revisited: Logging, agriculture, and biodiversity in Southeast Asia. Trends in Ecology & Evolution, 28(9): 531-540. https://doi.org/10.1016/j.tree.2013.04.005

[9] Global Forest Watch. (2023). Global Forest Watch data portal. World Resources Institute. https://www.globalforestwatch.org.

[10] Margono, B.A., Potapov, P.V., Turubanova, S., Stolle, F., Hansen, M.C. (2014). Primary forest cover loss in Indonesia over 2000–2012. Nature Climate Change, 4(8): 730-735. https://doi.org/10.1038/nclimate2277

[11] Wulder, M.A., Roy, D.P., Radeloff, V.C., Loveland, T.R., et al. (2022). Fifty years of Landsat science and impacts. Remote Sensing of Environment, 280: 113195. https://doi.org/10.1016/j.rse.2022.113195

[12] Gorelick, N., Hancher, M., Dixon, M., Ilyushchenko, S., Thau, D., Moore, R. (2017). Google Earth Engine: Planetary-scale geospatial analysis for everyone. Remote Sensing of Environment, 202: 18-27. https://doi.org/10.1016/j.rse.2017.06.031

[13] Tamiminia, H., Salehi, B., Mahdianpari, M., Quackenbush, L., Adeli, S., Brisco, B. (2020). Google Earth Engine for geo-big data applications: A meta-analysis and systematic review. ISPRS Journal of Photogrammetry and Remote Sensing, 164: 152-170. https://doi.org/10.1016/j.isprsjprs.2020.04.001

[14] White, R., Engelen, G. (1994). Urban systems dynamics

and cellular automata: Fractal structures between order and chaos. Chaos, Solitons & Fractals, 4(4): 563-583. https://doi.org/10.1016/0960-0779(94)90066-3

[15] Liu, X., Liang, X., Li, X., et al. (2017). A future land use simulation model (FLUS) for simulating multiple land use scenarios by coupling human and natural effects. Landscape and Urban Planning, 168: 94-116. https://doi.org/10.1016/j.landurbplan.2017.09.019

[16] Islam, K., Rahman, M.F., Jashimuddin, M. (2018). Modeling land use change using cellular automata and artificial neural network: The case of Chunati Wildlife Sanctuary, Bangladesh. Ecological Indicators, 88: 439-453. https://doi.org/10.1016/j.ecolind.2018.01.047

[17] Gharaibeh, A., Shaamala, A., Obeidat, R., Al-Kofahi, S. (2020). Improving land-use change modeling by integrating ANN with cellular automata-Markov chain model. Heliyon, 6(9): e05092. https://doi.org/10.1016/j.heliyon.2020.e05092

[18] Xu, T., Gao, J., Coco, G. (2019). Simulation of urban expansion via integrating artificial neural network with Markov chain–cellular automata. International Journal of Geographical Information Science, 33(10): 1960-1983. https://doi.org/10.1080/13658816.2019.1600701

[19] Sajan, B., Mishra, V.N., Kanga, S., Meraj, G., Singh, S.K., Kumar, P. (2022). Cellular automata-based artificial neural network model for assessing past, present, and future land use/land cover dynamics. Agronomy, 12(11): 2772. https://doi.org/10.3390/agronomy12112772

[20] Sangermano, F., Eastman, J.R., Zhu, H. (2010). Similarity weighted instance-based learning for the generation of transition potentials in land use change modeling. Transactions in GIS, 14(5): 569-580. https://doi.org/10.1111/j.1467-9671.2010.01226.x

[21] Pérez-Vega, A., Mas, J.F., Ligmann-Zielinska, A. (2012). Comparing two approaches to land use/cover change modeling and their implications for the assessment of biodiversity loss in a deciduous tropical forest. Environmental Modelling & Software, 29(1): 11-23. https://doi.org/10.1016/j.envsoft.2011.09.011

[22] e Silva, L.P., Xavier, A.P.C., da Silva, R.M., Santos, C.A.G. (2020). Modeling land cover change based on an artificial neural network for a semiarid river basin in northeastern Brazil. Global Ecology and Conservation, 21: e00811. https://doi.org/10.1016/j.gecco.2019.e00811

[23] Pontius Jr, R.G., Millones, M. (2011). Death to Kappa: Birth of quantity disagreement and allocation disagreement for accuracy assessment. International Journal of Remote Sensing, 32(15): 4407-4429. https://doi.org/10.1080/01431161.2011.552923

[24] Olmedo, M.T.C., Pontius Jr, R.G., Paegelow, M., Mas, J.F. (2015). Comparison of simulation models in terms of quantity and allocation of land change. Environmental Modelling & Software, 69: 214-221. https://doi.org/10.1016/j.envsoft.2015.03.003

[25] Pontius, G.R., Malanson, J. (2005). Comparison of the structure and accuracy of two land change models. International Journal of Geographical Information Science, 19(2): 243-265. https://doi.org/10.1080/13658810410001713434

[26] Hakim, A.M.Y., Baja, S., Rampisela, D.A., Arif, S. (2021). Modelling land use/land cover changes prediction using multi-layer perceptron neural network (MLPNN): A case study in Makassar City, Indonesia. International Journal of Environmental Studies, 78(2): 301-318. https://doi.org/10.1080/00207233.2020.1804730

[27] Saputra, M.H., Lee, H.S. (2019). Prediction of land use and land cover changes for North Sumatra, Indonesia, using an artificial-neural-network-based cellular automaton. Sustainability, 11(11): 3024. https://doi.org/10.3390/su11113024

[28] Leta, M.K., Demissie, T.A., Tränckner, J. (2021). Modeling and prediction of land use land cover change dynamics based on land change modeler (LCM) in Nashe watershed, Upper Blue Nile Basin, Ethiopia. Sustainability, 13(7): 3740. https://doi.org/10.3390/su13073740

[29] Tripathy, P., Kumar, A. (2019). Monitoring and modelling spatio-temporal urban growth of Delhi using cellular automata and geoinformatics. Cities, 90: 52-63. https://doi.org/10.1016/j.cities.2019.01.021

[30] Valencia, V.H., Levin, G., Hansen, H.S. (2020). Modelling the spatial extent of urban growth using a cellular automata-based model: A case study for Quito, Ecuador. Geografisk Tidsskrift-Danish Journal of Geography, 120(2): 156-173. https://doi.org/10.1080/00167223.2020.1823867

[31] Navarro Cerrillo, R.M., Palacios Rodríguez, G., Clavero Rumbao, I., Lara, M.Á., Bonet, F.J., Mesas-Carrascosa, F.J. (2020). Modeling major rural land-use changes using the GIS-based cellular automata Metronamica model: The case of Andalusia (Southern Spain). ISPRS International Journal of Geo-Information, 9(7): 458. https://doi.org/10.3390/ijgi9070458

[32] Laurance, W.F. (2013). Emerging threats to tropical forests. In Treetops at Risk: Challenges of Global Canopy Ecology and Conservation, pp. 71-79. https://doi.org/10.1007/978-1-4614-7161-5_5

[33] Malhi, Y., Gardner, T.A., Goldsmith, G.R., Silman, M.R., Zelazowski, P. (2014). Tropical forests in the Anthropocene. Annual Review of Environment and Resources, 39: 125-159. https://doi.org/10.1146/annurev-environ-030713-155141

[34] BPS Pasaman Regency. (2024). Pasaman Regency in Figures 2024. https://pasamankab.bps.go.id/en/publication/2024/02/28/dfaf9e708993f58d6f92ee04/kabupaten-pasaman-dalam-angka-2024.html.

[35] Bapedalda Provinsi Sumatera Barat. (2014). Buku data status lingkungan hidup daerah tahun 2014. https://www.scribd.com/document/323251546/Buku-Data-SLHD-Provinsi-Sumatera-Barat-Tahun-2014.

[36] Ramadhan, N., Dwipa, I., Muhsanati, M., et al. (2026). CHIRPS-based spatio-temporal rainfall analysis as a basis for evaluating cropping pattern suitability in coastal West Sumatra. Journal of Applied Agricultural Science and Technology, 10(1): 146-158. https://doi.org/10.55043/jaast.v10i1.524

[37] BPS Mapat Tunggul Selatan Sub-district. (2023). Mapat Tunggul Selatan Sub-district in Figures 2023. https://pasamankab.bps.go.id/en/publication/2023/09/26/74451608f971ca794484695c/mapat-tunggul-selatan-subdistrict-in-figures-2023.html.

[38] Keerthika, A., Lakshmi, P., Chavan, S.B., et al. (2024). Multistrata agroforestry systems: Spatial and temporal utilization of resources for higher production and better

income. In Agroforestry Solutions for Climate Change and Environmental Restoration, pp. 33-61. https://doi.org/10.1007/978-981-97-5004-7_2
[39] USGS. (2023). Landsat Collection 2 Level-2 science product guide. U.S. Geological Survey. https://www.usgs.gov/landsat-missions.
[40] Vermote, E., Justice, C., Claverie, M., Franch, B. (2016). Preliminary analysis of the performance of the Landsat 8/OLI land surface reflectance product. Remote Sensing of Environment, 185: 46-56. https://doi.org/10.1016/j.rse.2016.04.008
[41] Masek, J.G., Wulder, M.A., Markham, B., et al. (2020). Landsat 9: Empowering open science and applications through continuity. Remote Sensing of Environment, 248: 111968. https://doi.org/10.1016/j.rse.2020.111968
[42] Souza Jr, C.M., Shimbo, J.Z., Rosa, M.R., Parente, L.L., et al. (2020). Reconstructing three decades of land use and land cover changes in Brazilian biomes with Landsat archive and Earth Engine. Remote Sensing, 12(17): 2735. https://doi.org/10.3390/rs12172735
[43] Tassi, A., Gigante, D., Modica, G., Di Martino, L., Vizzari, M. (2021). Pixel-vs. object-based Landsat 8 data classification in Google Earth Engine using random forest: The case study of Maiella National Park. Remote Sensing, 13(12): 2299. https://doi.org/10.3390/rs13122299
[44] Basheer, S., Wang, X., Farooque, A.A., et al. (2022). Comparison of land use land cover classifiers using different satellite imagery and machine learning techniques. Remote Sensing, 14(19): 4978. https://doi.org/10.3390/rs14194978
[45] Olofsson, P., Foody, G.M., Herold, M., Stehman, S.V., Woodcock, C.E., Wulder, M.A. (2014). Good practices for estimating area and assessing accuracy of land change. Remote Sensing of Environment, 148: 42-57. https://doi.org/10.1016/j.rse.2014.02.015
[46] Olofsson, P., Foody, G.M., Stehman, S.V., Woodcock, C.E. (2013). Making better use of accuracy data in land change studies: Estimating accuracy and area and quantifying uncertainty using stratified estimation. Remote Sensing of Environment, 129: 122-131. https://doi.org/10.1016/j.rse.2012.10.031
[47] Wiwoho, B.S., Phinn, S., McIntyre, N. (2023). Two decades of land-use dynamics in an urbanizing tropical watershed: Understanding the patterns and drivers. ISPRS International Journal of Geo-Information, 12(3): 92. https://doi.org/10.3390/ijgi12030092
[48] Szabó, G., Singh, S.K., Szabó, S. (2015). Slope angle and aspect as influencing factors on the accuracy of the SRTM and the ASTER GDEM databases. Physics and Chemistry of the Earth, Parts A/B/C, 83: 137-145. https://doi.org/10.1016/j.pce.2015.06.003
[49] Anderson, J.R. (1976). A Land Use and Land Cover Classification System for Use with Remote Sensor Data (Vol. 964). US Government Printing Office. https://doi.org/10.3133/pp964
[50] Foody, G.M. (2002). Status of land cover classification accuracy assessment. Remote Sensing of Environment, 80(1): 185-201. https://doi.org/10.1016/S0034-4257(01)00295-4
[51] Austin, K.G., Mosnier, A., Pirker, J., McCallum, I., Fritz, S., Kasibhatla, P.S. (2017). Shifting patterns of oil palm driven deforestation in Indonesia and implications for zero-deforestation commitments. Land Use Policy, 69: 41-48. https://doi.org/10.1016/j.landusepol.2017.08.036
[52] Gaveau, D.L., Sheil, D., Husnayaen, et al. (2016). Rapid conversions and avoided deforestation: Examining four decades of industrial plantation expansion in Borneo. Scientific Reports, 6(1): 32017. https://doi.org/10.1038/srep32017
[53] Zhang, M., Liu, N., Harper, R., et al. (2017). A global review on hydrological responses to forest change across multiple spatial scales: Importance of scale, climate, forest type and hydrological regime. Journal of Hydrology, 546: 44-59. https://doi.org/10.1016/j.jhydrol.2016.12.040
[54] Laurance, W.F., Carolina Useche, D., Rendeiro, J., Kalka, M., et al. (2012). Averting biodiversity collapse in tropical forest protected areas. Nature, 489(7415): 290-294. https://doi.org/10.1038/nature11318
[55] Engert, J.E., Souza Jr, C.M., Kleinschroth, F., et al. (2025). Road expansion risk predicts future hotspots of tropical deforestation. Proceedings of the National Academy of Sciences, 122(52): e2502426122. https://doi.org/10.1073/pnas.2502426122
[56] Laurance, W.F., Goosem, M., Laurance, S.G. (2009). Impacts of roads and linear clearings on tropical forests. Trends in Ecology & Evolution, 24(12): 659-669. https://doi.org/10.1016/j.tree.2009.06.009
[57] Perz, S.G., Caldas, M.M., Arima, E., Walker, R.J. (2007). Unofficial road building in the Amazon: Socioeconomic and biophysical explanations. Development and Change, 38(3): 529-551. https://doi.org/10.1111/j.1467-7660.2007.00422.x
[58] Rafaai, N.H., Abdullah, S.A., Reza, M.I.H. (2020). Identifying factors and predicting the future land-use change of protected area in the agricultural landscape of Malaysian peninsula for conservation planning. Remote Sensing Applications: Society and Environment, 18: 100298. https://doi.org/10.1016/j.rsase.2020.100298
[59] Soares-Filho, B.S., Nepstad, D.C., Curran, L.M., et al. (2006). Modelling conservation in the Amazon basin. Nature, 440(7083): 520-523. https://doi.org/10.1038/nature04389
[60] Grinand, C., Vieilledent, G., Razafimbelo, T., Rakotoarijaona, J.R., Nourtier, M., Bernoux, M. (2020). Landscape-scale spatial modelling of deforestation, land degradation, and regeneration using machine learning tools. Land Degradation & Development, 31(13): 1699-1712. https://doi.org/10.1002/ldr.3526
[61] Kindu, M., Schneider, T., Döllerer, M., Teketay, D., Knoke, T. (2018). Scenario modelling of land use/land cover changes in Munessa-Shashemene landscape of the Ethiopian highlands. Science of the Total Environment, 622: 534-546. https://doi.org/10.1016/j.scitotenv.2017.11.338
[62] Bradshaw, C.J., Sodhi, N.S., Peh, K.S.H., Brook, B.W. (2007). Global evidence that deforestation amplifies flood risk and severity in the developing world. Global Change Biology, 13(11): 2379-2395. https://doi.org/10.1111/j.1365-2486.2007.01446.x
[63] Zhang, S., Deng, W., Zhang, H., Wang, Z. (2023). Identification and analysis of transitional zone patterns along urban-rural-natural landscape gradients: An application to China's southwest mountains. Land Use Policy, 129: 106625. https://doi.org/10.1016/j.landusepol.2023.106625
[64] IPCC. (2019). 2019 refinement to the 2006 IPCC

guidelines for national greenhouse gas inventories. Intergovernmental Panel on Climate Change. https://www.ipcc.ch/report/2019-refinement-to-the-2006-ipcc-guidelines-for-national-greenhouse-gas-inventories/.
[65] Pan, Y., Birdsey, R.A., Fang, J., Houghton, R., et al. (2011). A large and persistent carbon sink in the world's forests. Science, 333(6045): 988-993. https://doi.org/10.1126/science.1201609
[66] Republic of Indonesia. (2021). Updated nationally determined contribution. Ministry of Environment and Forestry, Jakarta. https://unfccc.int/sites/default/files/NDC/2022-06/Updated%20NDC%20Indonesia%202021%20-%20corrected%20version.pdf.